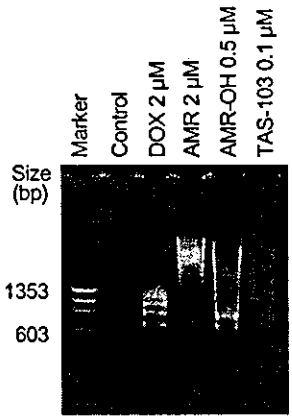

Fig. 9. Detection of DNA ladder formation in HL-60 cells treated with DOX, AMR, AMR-OH and TAS-103. HL-60 cells (1×10^6 cells/ml) were treated with reagents at 37 °C for 8 h. The cells were lysed, and DNA was extracted and analyzed by conventional electrophoresis. Marker lane: size marker DNA (ΦX174/*Hae* III digest).

(AMR and TAS-103) in the presence of Cu(II). AMR is a new anthracycline antibiotic and TAS-103 is a topoisomerase I and II inhibitor (Utsugi et al., 1997; Hanada et al., 1998; Mizutani et al., 2002). DOX, AMR and AMR-OH (an active metabolite of AMR) caused DNA damage in the presence of Cu(II), but TAS-103 did not (Fig. 8). DOX, AMR, AMR-OH and TAS-103 did not cause DNA damage in the absence of Cu(II). The order of ability of DNA damage in the presence of Cu(II) was DOX > AMR, AMR-OH >> TAS-103 (Fig. 8).

DNA ladder formation in HL-60 cells treated with DOX, AMR, AMR-OH and TAS-103

Since the ability of DNA damage induced by DOX, AMR, AMR-OH and TAS-103 is different, we compared DNA ladder formation in HL-60 cells treated with DOX, AMR, AMR-OH and TAS-103. Each agent induced DNA ladder formation in HL-60 cells. The order of ability of DNA ladder formation was TAS-103 > AMR-OH > DOX, AMR (Fig. 9).

Discussion

The present study showed that DOX induced apoptosis in both HL-60 cells and the H_2O_2-resistant clone, HP100 cells. The apparent DNA ladder formation could be detected at above 1 μM in HL-60 cells after an 8 h incubation, whereas it could be detected at above 2 μM in HP-100 cells. In HP100 cells, DNA ladder formation, H_2O_2 generation, $\Delta\Psi m$ increase and caspase-3 activation were delayed, compared with those of HL-60 cells. H_2O_2 formation preceded the $\Delta\Psi m$ increase and caspase-3 activation in DOX-induced apoptosis; in HL-60 cells, H_2O_2 generation occurred at 1 h, followed by the $\Delta\Psi m$ increase at 4 h, whereas in HP100 cells, H_2O_2 generation was completely suppressed at 1 and 2 h, and the $\Delta\Psi m$ increase occurred at 6 h. The caspase-3 activity in HL-60 was significantly higher than that in HP100 at 8 h. It was reported that HP100 cells are about 340-fold more resistant to H_2O_2 than the parent cells, HL-60 (Kasugai and Yamada, 1992). Therefore, these findings can be explained by the involvement of H_2O_2 generation in the DOX-induced apoptotic pathway.

Here, the question has been raised how DOX induces the intracellular H_2O_2 generation. Firstly, the redox-cycle of DOX should be considered as the source of H_2O_2, since DOX has both the para-quinone and para-hydroquinone residues. DOX can react at the quinone residue with cytochrome P450 reductase in the presence of NADPH to form the semiquinone radical via a one-electron reduction, resulting in generation of H_2O_2 (Gewirtz, 1999; Jung and Reszka, 2001). H_2O_2 generation is also caused by the oxidative activation of DOX, that is, a one-electron oxidation of para-OH residue (Pietronigro et al., 1979; Chinami et al., 1984; Reszka et al., 2001; Mizutani et al., 2003). Therefore, the H_2O_2 generation can be initiated by reduction or oxidation of DOX, this H_2O_2 generation mediates oxidative DNA damage (Berlin and Haseltine, 1981; Gewirtz, 1999; Jung and Reszka, 2001; Mizutani et al., 2003). In the present experiment, DOX significantly induced 8-oxodG formation in HL-60, but not in HP100, suggesting that the oxidative DNA damage was induced by the H_2O_2 generation.

Secondly, there is a possibility that the NAD(P)H oxidase activation mediates H_2O_2 generation. We reported a new apoptotic mechanism as follows: DNA cleavage by a topoisomerase inhibitor, which cannot directly generate H_2O_2 by itself, induces PARP hyperactivation and subsequent depletion of both NAD^+ and $NADP^+$ in cells treated with the topoisomerase inhibitor may result in the activation of NAD(P)H oxidase to maintain the cellular redox balance by converting NAD(P)H to $NAD(P)^+$. NAD(P)H oxidase catalyzes the following reaction: $NAD(P)H + 2O_2 \rightarrow 2O_2^- + NAD(P)^+ + H^+$. O_2^- is then rapidly converted to H_2O_2. This O_2^--derived H_2O_2 generation, followed by the $\Delta\Psi m$ increase and subsequent caspase-3 activation, leads to apoptosis (Mizutani et al., 2002). In the present study, DOX-induced DNA ladder formation was prevented by PARP inhibitors and NAD(P)H oxidase inhibitors, indicating that DOX-mediated apoptosis occurs through PARP activation and subsequent NAD(P)H oxidase activation. Oxidative DNA damage as well as DNA cleavage hyperactivates PARP (Vrag and Szabo, 2002). In addition, many reports have presented that DOX-induced oxidative stress is related to cardiotoxicity and cardiomyocyte apoptosis (Gewirtz, 1999; De Beer et al., 2001; Childs et al., 2002; Green and Leeuwenburgh, 2002). PARP suppression by genetic deletion and a PARP inhibitor depressed DOX-induced cardiotoxicity (Pacher et al., 2002). These reports support the idea that DOX-induced oxidative DNA damage hyperactivates PARP. On the other hand, DOX-induced H_2O_2 generation and change of $\Delta\Psi m$ were not suppressed by ANI, a PARP inhibitor, suggesting that the redox-cycle of DOX may be the main source of H_2O_2 generation in an early stage of apoptotic process, leading to 8-oxodG formation. In the present study, DPI decreased DOX-induced H_2O_2 generation, suggesting that DPI may inhibit NADPH-cytochrome P450 redutase, resulting in suppression of enzymatic DOX reduction-dependent H_2O_2 generation (Tew, 1993; Ramji et al., 2003). DPI increased DOX-induced change of $\Delta\Psi m$. The observation may be explained by assuming that DPI induces mitochondrial dysfunction (Li et al., 2003).

Topoisomerase II is one of the primary target sites for the activity of the anthracycline antibiotics. The previous reports have presented that DOX causes DNA cleavage induced by topoisomerase II inhibition (Tewey et al., 1984; Gewirtz, 1999; Hurley, 2002), whereas we have demonstrated that DOX causes oxidative DNA damage in the presence of Cu(II) (Mizutani et al., 2003). The present study performed that the order of ability of DNA damage in the presence of Cu(II) was DOX > AMR-OH >> TAS-103. This result is consistent with the finding that TAS-103-induced DNA cleavage is not mediated by oxidative stress (Mizutani et al., 2002). On the other hand, AMR-OH and TAS-103 cause DNA cleavage mediated by formation of cleavable complex (Utsugi et al., 1997; Hanada et al., 1998; Padget et al., 2000), whereas DOX does not form

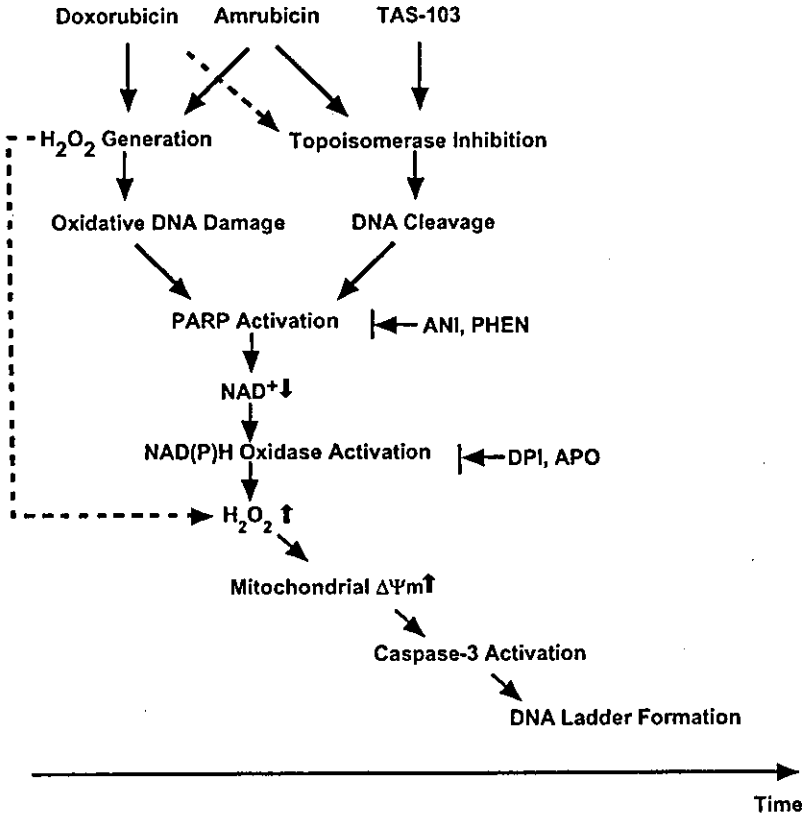

Fig. 10. Possible mechanisms of apoptosis by anticancer drugs.

cleavable complex (Hanada et al., 1998). This study showed that the order of ability of DNA ladder formation was TAS-103 > AMR-OH > DOX. According to these observations and references, we proposed two different mechanisms of apoptosis by anticancer drugs as shown in Fig. 10. TAS-103 induces apoptosis through topoisomerase inhibition and subsequent indirect H_2O_2 generation. AMR-OH-induced apoptosis involves both oxidative DNA damage and topoisomerase II inhibition. DOX-induced apoptosis is mainly initiated by oxidative DNA damage mediated by H_2O_2, which is directly generated from redox-cycle, although this apoptosis may involve topoisomerase II inhibition. This oxidative DNA damage mediates indirect H_2O_2 generation through PARP and NAD(P)H oxidase activation, leading to the $\Delta\Psi m$ increase and subsequent caspase-3 activation in DOX-induced apoptosis.

Acknowledgments

This work was supported by Grants-in-Aid for Scientific Research from the Ministry of Education, Culture, Sports, Science and Technology of Japan.

References

Berlin, V., Haseltine, W.A., 1981. Reduction of adriamycin to a semiquinone-free radical by NADPH cytochrome P-450 reductase produces DNA cleavage in a reaction mediated by molecular oxygen. Journal of Biological Chemistry 256, 4747–4756.

Bertrand, R., Solary, E., Jenkins, J., Pommier, Y., 1993. Apoptosis and its modulation in human promyelocytic HL-60 cells treated with DNA topoisomerase I and II inhibitors. Experimental Cell Research 207, 388–397.

Chabner, B.A., Allegra, C.J., Curt, G.A., Calabresi, P., 1996. Antineoplastic agents. In: Hardman, J.G., Limbird, L.E. (Eds.), Goodman and Gilman's the Pharmacological Basis of Therapeutics, 9th ed. McGraw-Hill, New York, pp. 1233–1287.

Chandra, J., Samali, A., Orrenius, S., 2000. Triggering and modulation of apoptosis by oxidative stress. Free Radical Biology and Medicine 29, 323–333.

Childs, A.C., Phaneuf, S.L., Dirks, A.J., Phillips, T., Leeuwenburgh, C., 2002. Doxorubicin treatment in vivo causes cytochrome C release and cardiomyocyte apoptosis, as well as increased mitochondrial efficiency, superoxide dismutase activity, and Bcl-2:Bax ratio. Cancer Research 62, 4592–4598.

Chinami, M., Kato, T., Ogura, R., Shingu, M., 1984. Semiquinone formation of adriamycin by oxidation at para-OH residue. Biochemistry International 8, 299–304.

Costantini, P., Jacotot, E., Decaudin, D., Kroemer, G., 2000. Mitochondrion as a novel target of anticancer chemotherapy. Journal of the National Cancer Institute 92, 1042–1053.

De Beer, E.L., Bottone, A.E., Voest, E.E., 2001. Doxorubicin and mechanical performance of cardiac trabeculae after acute and chronic treatment: a review. European Journal of Pharmacology 415, 1–11.

Decaudin, D., Geley, S., Hirsch, T., Castedo, M., Marchetti, P., Macho, A., Kofler, R., Kroemer, G., 1997. Bcl-2 and Bcl-XL antagonize the mitochondrial dysfunction preceding nuclear apoptosis induced by chemotherapeutic agents. Cancer Research 57, 62–67.

Green, P.S., Leeuwenburgh, C., 2002. Mitochondrial dysfunction is an early indicator of doxorubicin-induced apoptosis. Biochimica et Biophysica Acta 1588, 94–101.

Gewirtz, D.A., 1999. A critical evaluation of the mechanisms of action proposed for the antitumor effects of the anthracycline antibiotics adriamycin and daunorubicin. Biochemical Pharmacology 57, 727–741.

Gottlieb, R.A., 2000. Mitochondria: execution central. FEBS Letters 482, 6–12.

Hampton, M.B., Fadeel, B., Orrenius, S., 1998. Redox regulation of the caspases during apoptosis. Annals of the New York Academy of Sciences 854, 328–335.

Hanada, M., Mizuno, S., Fukushima, A., Saito, Y., Noguchi, T., Yamaoka, T., 1998. A new antitumor agent amrubicin induces cell growth inhibition by stabilizing topoisomerase II-DNA complex. Japanese Journal of Cancer Research 89, 1229–1238.

Hiraku, Y., Kawanishi, S., 1996. DNA damage and apoptosis induced by benzene metabolites. Cancer Research 56, 5172–5178.

Hishita, T., Tada-Oikawa, S., Tohyama, K., Miura, Y., Nishihara, T., Tohyama, Y., Yoshida, Y., Uchiyama, T., Kawanishi, S., 2001. Caspase-3 activation by lysosomal enzymes in cytochrome c-independent apoptosis in myelodysplastic syndrome-derived cell line P39. Cancer Research 61, 2878–2884.

Hurley, L.H., 2002. DNA and its associated processes as targets for cancer therapy. Nature Reviews Cancer 2, 188–200.

Ikeda, K., Kajiwara, K., Tanabe, E., Tokumaru, S., Kishida, E., Masuzawa, Y., Kojo, S., 1999. Involvement of hydrogen peroxide and hydroxyl radical in chemically induced apoptosis of HL-60 cells. Biochemical Pharmacology 57, 1361–1365.

Ito, K., Inoue, S., Yamamoto, K., Kawanishi, S., 1993. 8-Hydroxydeoxyguanosine formation at the 5′ site of 5′ -GG-3′ sequences in double-stranded DNA by UV radiation with riboflavin. Journal of Biological Chemistry 268, 13221–13227.

Jones, R.D., Hancock, J.T., Morice, A.H., 2000. NADPH oxidase: a universal oxygen sensor? Free Radical Biology and Medicine 29, 416–424.

Jung, K., Reszka, R., 2001. Mitochondria as subcellular targets for clinically useful anthracyclines. Advanced Drug Delivery Reviews 49, 87–105.

Kajiwara, K., Ikeda, K., Kuroi, R., Hashimoto, R., Tokumaru, S., Kojo, S., 2001. Hydrogen peroxide and hydroxyl radical involvement in the activation of caspase-3 in chemically induced apoptosis of HL-60 cells. Cellular and Molecular Life Sciences 58, 485–491.

Kasugai, I., Yamada, M., 1989. Adaptation of human leukemia HL-60 cells to hydrogen peroxide as oxidative stress. Leukemia Research 13, 757–762.

Kasugai, I., Yamada, M., 1992. High production of catalase in hydrogen peroxide-resistant human leukemia HL-60 cell lines. Leukemia Research 16, 173–179.

Kaufmann, S.H., Earnshaw, W.C., 2000. Induction of apoptosis by cancer chemotherapy. Experimental Cell Research 256, 42–49.

Kroemer, G., Zamzami, N., Susin, S.A., 1997. Mitochondrial control of apoptosis. Immunology Today 18, 44–51.

Kroemer, G., Reed, J.C., 2000. Mitochondrial control of cell death. Nature Medicine 6, 513–519.

Li, N., Ragheb, K., Lawler, G., Sturgis, J., Rajwa, B., Melendez, J.A., Robinson, J.P., 2003. DPI induces mitochondrial superoxide-mediated apoptosis. Free Radical Biology and Medicine 34, 465–477.

Martin, D.S., Bertino, J.R., Koutcher, J.A., 2000. ATP depletion + pyrimidine depletion can markedly enhance cancer therapy: fresh insight for a new approach. Cancer Research 60, 6776–6783.

Mignotte, B., Vayssiere, J.L., 1998. Mitochondria and apoptosis. European Journal of Biochemistry 252, 1–15.

Mizutani, H., Tada-Oikawa, S., Hiraku, Y., Oikawa, S., Kojima, M., Kawanishi, S., 2002. Mechanism of apoptosis induced by a new topoisomerase inhibitor through the generation of hydrogen peroxide. Journal of Biological Chemistry 277, 30684–30689.

Mizutani, H., Oikawa, S., Hiraku, Y., Murata, M., Kojima, M., Kawanishi, S., 2003. Distinct mechanisms of site-specific oxidative DNA damage by doxorubicin in the presence of copper (II) and NADPH-cytochrome P450 reductase. Cancer Science 94, 686–691.

Muller, I., Niethammer, D., Bruchelt, G., 1998. Anthracycline-derived chemotherapeutics in apoptosis and free radical cytotoxicity. International Journal of Molecular Medicine 1, 491–494.

Nakagawa, Y., Akao, Y., Morikawa, H., Hirata, I., Katsu, K., Naoe, T., Ohishi, N., Yagi, K., 2002. Arsenic trioxide-induced apoptosis through oxidative stress in cells of colon cancer cell lines. Life Sciences 70, 2253–2269.

Pacher, P., Liaudet, L., Bai, P., Virag, L., Mabley, J.G., Hasko, G., Szabo, C., 2002. Activation of poly(ADP-ribose) polymerase contributes to development of doxorubicin-induced heart failure. Journal of Pharmacology and Experimental Therapeutics 300, 862–867.

Padget, K., Stewart, A., Charlton, P., Tilby, M.J., Austin, C.A., 2000. An investigation into the formation of N-[2-(dimethylamino)ethyl]acridine-4-carboxamide (DACA) and 6-[2-(dimethylamino)ethylamino]-3-hydroxy-7H-indeno[2, 1-C]quinolin-7-one dihydrochloride (TAS-103) stabilised DNA topoisomerase I and II cleavable complexes in human leukaemia cells. Biochemical Pharmacology 60, 817–821.

Pietronigro, D.D., McGinness, J.E., Koren, M.J., Crippa, R., Seligman, M.L., Demopoulos, H.B., 1979. Spontaneous generation of adriamycin semiquinone radicals at physiologic pH. Physiological Chemistry and Physics 11, 405–414.

Ramji, S., Lee, C., Inaba, T., Patterson, A.V., Riddick, D.S., 2003. Human NADPH-cytochrome P450 reductase overexpression does not enhance the aerobic cytotoxicity of doxorubicin in human breast cancer cell lines. Cancer Research 63, 6914–6919.

Reszka, K.J., McCormick, M.L., Britigan, B.E., 2001. Peroxidase- and nitrite-dependent metabolism of the anthracycline anticancer agents daunorubicin and doxorubicin. Biochemistry 40, 15349–15361.

Scovassi, A.I., Poirier, G.G., 1999. Poly(ADP-ribosylation) and apoptosis. Molecular and Cellular Biochemistry 199, 125–137.

Sellers, W.R., Fisher, D.E., 1999. Apoptosis and cancer drug targeting. Journal of Clinical Investigation 104, 1655–1661.

Tada-Oikawa, S., Oikawa, S., Kawanishi, M., Yamada, M., Kawanishi, S., 1999. Generation of hydrogen peroxide precedes loss of mitochondrial membrane potential during DNA alkylation-induced apoptosis. FEBS Letters 442, 65–69.

Tew, D.G., 1993. Inhibition of cytochrome P450 reductase by the diphenyliodonium cation. Kinetic analysis and covalent modifications. Biochemistry 32, 10209–10215.

Tewey, K.M., Rowe, T.C., Yang, L., Halligan, B.D., Liu, L.F., 1984. Adriamycin-induced DNA damage mediated by mammalian DNA topoisomerase II. Science 226, 466–468.

Tsang, W.P., Chau, S.P., Kong, S.K., Fung, K.P., Kwok, T.T., 2003. Reactive oxygen species mediate doxorubicin induced p53-independent apoptosis. Life Sciences 73, 2047–2058.

Utsugi, T., Aoyagi, K., Asao, T., Okazaki, S., Aoyagi, Y., Sano, M., Wierzba, K., Yamada, Y., 1997. Antitumor activity of a novel quinoline derivative, TAS-103, with inhibitory effects on topoisomerases I and II. Japanese Journal of Cancer Research 88, 992–1002.

Vrag, L., Szabo, C., 2002. The therapeutic potential of poly(ADP-ribose)polymerase inhibitors. Pharmacological Reviews 54, 375–429.

Xiang, J., Chao, D.T., Korsmeyer, S.J., 1996. BAX-induced cell death may not require interleukin 1β-converting enzyme-like proteases. Proceedings of the National Academy of Sciences of the United States of America 93, 14559–14563.

Available online at www.sciencedirect.com
SCIENCE DIRECT®
Archives of Biochemistry and Biophysics 434 (2005) 232–240
ABB
www.elsevier.com/locate/yabbi

Amplification of C1027-induced DNA cleavage and apoptosis by a quinacrine–netropsin hybrid molecule in tumor cell lines☆

Takuya Iwamoto[a,b], Yusuke Hiraku[a], Michio Kojima[b], Shosuke Kawanishi[a,*]

[a] *Department of Environmental and Molecular Medicine, Mie University School of Medicine, 2-174 Edobashi, Tsu, Mie 514 8507, Japan*
[b] *Department of Pharmacy, Mie University Hospital, Tsu, Mie 514 8507, Japan*

Received 20 August 2004, and in revised form 12 November 2004
Available online 2 December 2004

Abstract

We examined the effect of a newly synthesized DNA-binding ligand, quinacrine–netropsin hybrid molecule (QN), on cytotoxicity, apoptosis, and DNA strand breaks induced by an enediyne antitumor antibiotic, C1027. QN significantly enhanced C1027-induced cellular DNA strand breaks, caspase-3 activation, and DNA ladder formation, characteristic of apoptosis, in human HL-60 cells. Flow cytometry revealed that C1027-induced intracellular H_2O_2 generation was enhanced by QN, suggesting that QN enhances C1027-induced cytotoxic effect through H_2O_2-mediated apoptosis. QN also significantly enhanced C1027-induced apoptosis in BJAB cells, and the inhibition of apoptosis was observed in BJAB cells transfected with Bcl-2 gene. The experiment using ^{32}P-labeled DNA fragments showed that the addition of QN enhanced C1027-induced double-stranded DNA cleavage at the 5′-AGG-3′/3′-TCC-5′ sequence (cutting sites are underlined). These results suggest that QN enhances C1027-induced antitumor effect via DNA cleavage and apoptosis. The present study shows a novel approach to the potentially effective anticancer therapy.

Keywords: C1027; Enediyne; DNA-binding ligand; Apoptosis; Site specificity

DNA is the molecular target for a number of antitumor drugs [1]. Such antitumor drugs exert their effect by inducing apoptosis following DNA damage [2–5]. Recently, much effort has been put into finding a new cancer therapy with greater sensitivity and less toxicity, because most of the antitumor drugs cause severe side effects. In particular, it is a very attractive idea that DNA-binding ligands, which recognize specific base sequences, could amplify the activity of antitumor drugs [6–8]. Application of DNA-binding ligands to cancer therapies may enable to reduce anticancer drug doses and its unwanted side effects, which occur dose-dependently and independently of DNA damage. We have previously demonstrated that antitumor drug-induced DNA cleavage was enhanced by DNA-binding ligands, such as minor groove binders [9–11] and intercalators [8,12]. Particularly, certain unfused aromatic cations intercalating into DNA dramatically amplified bleomycin-induced apoptosis [8].

C1027, an enediyne antitumor antibiotic, containing an apoprotein and a chromophore, showed extremely potent cytotoxicity by causing DNA strand breaks [13] and markedly inhibited the growth of transplantable tumors in mice [14]. The enediyne moiety of the chromophore spontaneously undergoes rearrangement to form a highly reactive benzenoid diradical species (Fig. 1). This species, positioned in the DNA minor groove, abstracts hydrogen atoms from the deoxyribose of the backbone, resulting in double-strand breaks with a two-nucleotide 3′-stagger of the cleaved residues, particularly

☆ This work was supported by Grants-in-Aid for Scientific Research granted by the Ministry of Education, Science, Sports and Culture of Japan.
* Corresponding author. Fax: +81 59 231 5011.
E-mail address: kawanisi@doc.medic.mie-u.ac.jp (S. Kawanishi).

0003-9861/$ - see front matter © 2004 Elsevier Inc. All rights reserved.
doi:10.1016/j.abb.2004.11.017

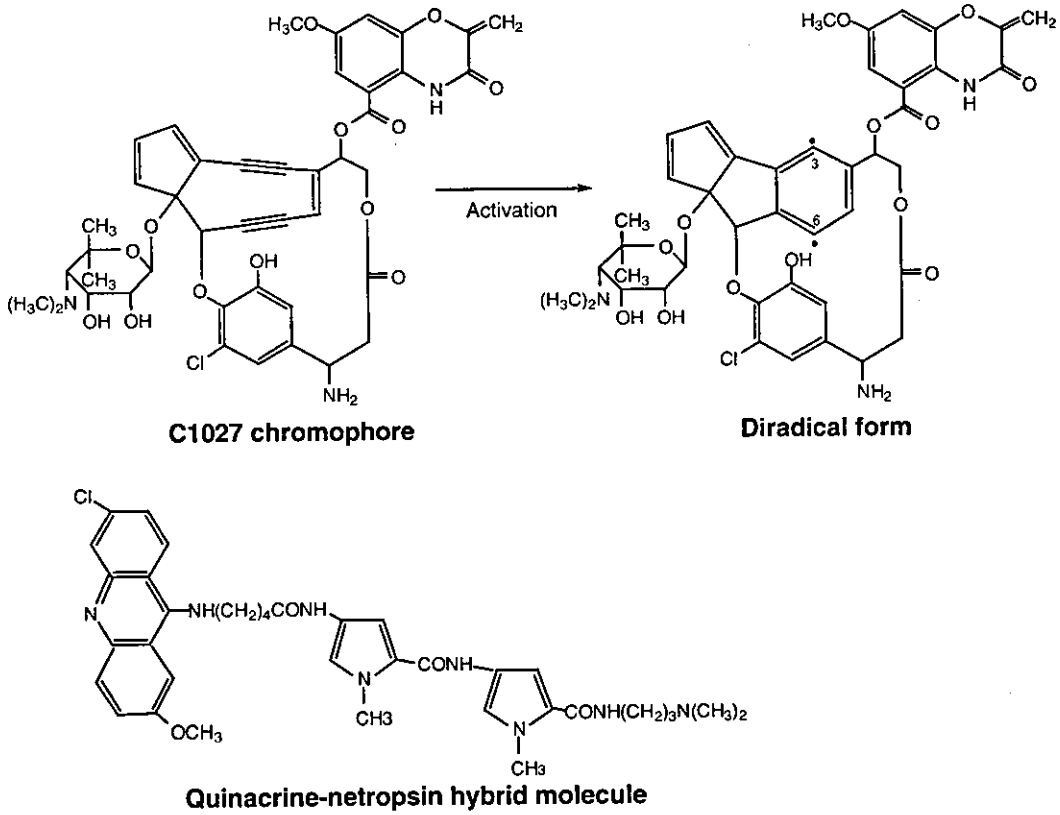

Fig. 1. Chemical structures of C1027 and QN.

at AT-rich sequences [15,16]. One of the enediyne antitumor antibiotics, neocarzinostatin, induced DNA cleavage [17,18], and its site specificity was changed by actinomycin D, an intercalator of DNA [12]. Therefore, the site specificity and intensity of C1027-induced DNA cleavage might be changed depending on interactions between drug molecules and DNA microstructure, resulting in enhancement of its cytotoxicity.

In this study, we used a newly synthesized quinacrine–netropsin hybrid molecule (QN)[1] (Fig. 1), as a DNA-binding ligand to enhance C1027-induced antitumor effect. Quinacrine is highly permeable to cell membrane [19] and intercalates into DNA [20,21]. Netropsin has been reported to bind to DNA at AT-rich sequences in the minor groove [22,23]. QN may effectively enhance the antitumor activity of C1027 through intermolecular reaction with DNA. We investigated the effect of QN on C1027-induced cytotoxicity, cellular DNA strand breaks, and internucleosomal DNA fragmentation, which is characteristic of apoptosis. We also performed flow cytometry to examine intracellular H_2O_2 generation by C1027 and QN, since we have previously found that antitumor drug-induced DNA strand breaks mediate generation of H_2O_2, leading to apoptosis [2,4]. Furthermore, we determined the alteration in the site specificity of C1027-induced DNA cleavage by addition of QN using ^{32}P-5′- and ^{32}P-3′-end-labeled DNA fragments obtained from the human c-Ha-*ras*-1 proto-oncogene.

Materials and methods

Materials

QN, a gift from Prof. Yukio Kubota (Yamaguchi University), was synthesized according to the procedures described in the literature [24,25]. The data of elemental analysis (C, H, and N) of QN were in agreement with calculated values and its spectroscopic data (1H nuclear magnetic resonance and mass spectrum) were consistent with the assigned structure. C1027 was kindly provided by Taiho Pharmaceutical (Tokyo, Japan). Proteinase K was from Boehringer–Mannheim GmbH (Mannheim, Germany). Restriction enzymes (*Ava*I and *Pst*I) and T_4 polynucleotide kinase were purchased from New England Biolabs (Beverly, MA, USA). [γ-^{32}P]ATP and [α-^{32}P]ATP were from New England Nuclear (Boston, MA, USA). The Klenow fragment of DNA polymerase I of *Escherichia coli* was from Takara Shuzo (Otsu,

[1] *Abbreviations used:* QN, synthesized quinacrine–netropsin hybrid molecule; Chaps, 3-[(3-cholamidopropyl)dimethylammonio]-1-propanesulfonic acid; DEVD-AFC, Ac-Asp-Glu-Val-Asp-7-amino-4-trifluoromethyl coumarin; DCFH-DA, 2′,7′-dichlorofluorescin diacetate; DTPA, diethylenetriamine-*N*,*N*,*N*′,*N*″,*N*″-pentaacetic acid; PBS, phosphate-buffered saline; FCS, fetal calf serum.

Japan). Quinacrine, dithiothreitol, and G418 were from Nacalai Tesque (Kyoto, Japan). Netropsin, RNase, and 3-[(3-cholamidopropyl)dimethylammonio]-1-propanesulfonic acid (Chaps) were from Sigma Chemical (St. Louis, MO, USA). Propidium iodide, 2′,7′-dichlorofluorescin diacetate (DCFH-DA), and Ac-Asp-Glu-Val-Asp-7-amino-4-trifluoromethyl coumarin (DEVD-AFC) were from Molecular Probes (Eugene, OR, USA). Hoechst 33258 was from Polysciences (Warrington, PA, USA). Diethylenetriamine-*N*,*N*,*N*′,*N*″,*N*″-pentaacetic acid (DTPA) was from Dojin Chemicals (Kumamoto, Japan).

Cell culture

HL-60 and HP100 cells were grown in RPMI 1640 (Gibco Laboratories, NY) supplemented with 6% fetal calf serum (FCS, Whittaker Bioproducts) at 37 °C under 5% CO_2 in a humidified atmosphere. HP100 cells were created from HL-60 cells by repeated exposure to 100 μM H_2O_2. The outgrowth of viable cells resulted in HP100 cells, ~340-fold more resistant to H_2O_2 than the parental cell line, HL-60 [26]. Catalase activity in HP100 cells is 18-fold higher than in HL-60 cells.

Human B-lymphoma cell line, BJAB cells, was grown in RPMI 1640 medium supplemented with 6% FCS and 0.5 mg/ml G418. The BJAB cells were co-transfected with the pCAGGS plasmid carrying the Bcl-2 gene and the PCMVneo plasmid carrying the neomycin-phosphotransferase resistance gene (BJAB/Bcl-2 cells) as described previously [4]. The cells carrying the neomycin-phosphotransferase gene without the Bcl-2 gene (BJAB/neo cells) were produced by a similar method.

C1027-induced cytotoxicity in the presence of QN

Cells (5×10^5 cells/ml) were incubated with C1027 and QN in 2 ml medium and harvested at indicated time. Cell viability was determined by trypan blue staining. To detect apoptotic cells, cells were stained with 50 μM Hoechst 33258 and 10 μM propidium iodide for 10 min. Nuclei of viable, necrotic, and apoptotic cells were observed as blue intact nuclei, red intact nuclei, and fragmented or condensed nuclei, respectively [27]. For statistical analysis of the data, independent *t* test was used at a significance level of $p < 0.05$. The data represent means ± SD of three independent experiments.

Detection of cellular DNA strand breaks induced by C1027 in the presence of QN

HL-60 cells (5×10^5 cells/ml) were treated with QN and C1027 in 2 ml medium for 10 min at 37 °C, and then washed twice with phosphate-buffered saline (PBS). Cell suspensions were solidified with agarose, followed by treatment with proteinase K according to the method described previously [28]. Electrophoresis was performed at 14 °C using a CHEF-DRII pulse field electrophoresis system (Bio-Rad) at 200 V. Switch time was 60 s for 15 h followed by 90 s for 9 h. The DNA in the gel was visualized using ethidium bromide.

Detection of internucleosomal DNA fragmentation induced by C1027 in the presence of QN

HL-60 cells (5×10^5 cells/ml) were treated with QN and C1027 in 2 ml medium for 2 h at 37 °C, and then washed twice with PBS. Cells were lysed and treated with RNase and proteinase K as described previously [29]. The DNA was then electrophoresed on 1.4% agarose gel containing ethidium bromide.

Flow cytometric detection of peroxide in cultured cells treated with C1027 and QN

To evaluate cellular peroxide levels, HL-60 and HP100 cells (5×10^5 cells/ml) were treated with 50 pM C1027, 1 μM QN, and 5 μM DCFH-DA in 2 ml medium for 30 min at 37 °C [30]. Cells were then washed once with PBS. Following resuspension in PBS, the cells were analyzed on a flow cytometer (FACScan; Becton Dickinson, San Jose, CA). Dead cells and debris were excluded from the analysis. The data were analyzed using Cell Quest software (Becton Dickinson).

Measurement of caspase-3 activity

Caspase-3 activity was measured as described previously [4]. HL-60 cells (5×10^5 cells/ml) were treated with 50 pM C1027 and 1 μM QN in 2 ml medium for 2 h at 37 °C. Cells were then washed twice with PBS and resuspended in 100 μl assay buffer containing 0.1 M Hepes (pH 7.4), 2 mM dithiothreitol, 0.1% Chaps, and 1% sucrose. Cell suspensions were frozen in liquid nitrogen and then thawed at 37 °C. This freeze–thaw procedure was repeated three times. Cell lysates were then centrifuged at 18,000*g* for 20 min, to obtain the apoptotic extracts. Reaction was initiated by the addition of 20 μM DEVD-AFC, a caspase-3 substrate, to the apoptotic extract diluted with the freshly prepared assay buffer at 37 °C. AFC was measured using a Shimazu FC 5300 spectrofluorometer with excitation at 400 nm and emission at 505 nm.

Preparation of ^{32}P-5′-labeled DNA fragments from the c-Ha-ras-1 proto-oncogene

DNA fragments were prepared from plasmid pbcNI, which carries a 6.6-kb *Bam*HI chromosomal DNA segment containing the human c-Ha-*ras*-1 proto-oncogene [31,32]. The 435-bp fragment (*Ava*I 2247–*Ava*I 2681) was labeled at 5′ end with [γ-^{32}P]ATP, and 98-bp fragment

(*Ava*I* 2247–*Pst*I 2344), and 337-bp fragment (*Pst*I 2345–*Ava*I* 2681) were obtained according to the method described previously [31,32]. The asterisk indicates ^{32}P-labeling and nucleotide numbering starts with the *Bam*HI site [33].

Preparation of ^{32}P-3′-labeled DNA fragments from the c-Ha-ras-1 proto-oncogene

The 435-bp fragment (*Ava*I 2247–*Ava*I 2681) was treated with 0.1 U Klenow fragment and [α-^{32}P]ATP for 2.5 h at 37 °C. Then, the fragment was digested with 50 U *Pst*I for 1.5 h at 37 °C to obtain the ^{32}P-3′-labeled 337-bp fragment (*Pst*I 2345–*Ava*I* 2681). DNA fragment was purified by electrophoresis.

Detection of damage to isolated DNA induced by C1027 in the presence of DNA-binding ligands

The standard reaction mixture (in a 1.5 ml Eppendorf microtube) contained ^{32}P-end-labeled DNA fragments, calf thymus DNA (10 μM/base), 0.1 nM C1027, and indicated concentration of DNA-binding ligands, quinacrine, netropsin or QN, in 200 μl of 10 mM sodium phosphate buffer (pH 7.8), containing 5 μM DTPA. After incubation for 30 min at 37 °C, the treated DNA fragments were electrophoresed and the autoradiogram was obtained by exposing X-ray film to the gel as described previously [34]. The preferred cleavage sites were determined by direct comparison of the positions of the oligonucleotides with those produced by the chemical reactions of the Maxam–Gilbert procedure [35] using a DNA-sequencing system (LKB 2010 Macrophor, Pharmacia Biotech, Uppsala, Sweden). The relative amounts of oligonucleotides from the treated DNA fragments were measured with a laser densitometer (Personal Densitometer SI, Amarsham Biosciences).

Results

Cytotoxic effect of C1027 in the presence of QN

We examined the effect of QN on C1027-induced cytotoxicity in human HL-60 cells. QN significantly enhanced C1027-induced cytotoxicity after the 1 h treatment ($p < 0.05$) (Fig. 2A), although quinacrine or netropsin alone did not affect the cytotoxicity of C1027 (data not shown). The cells with fragmented and condensed chromatin were defined as apoptotic cells in Hoechst 33258 and propidium iodide staining. This morphologic analysis showed that QN significantly increased the apoptotic cell number in comparison with C1027 alone after the 1 h treatment ($p < 0.05$) (Fig. 2B). QN alone showed no cytotoxic effect under the condition used.

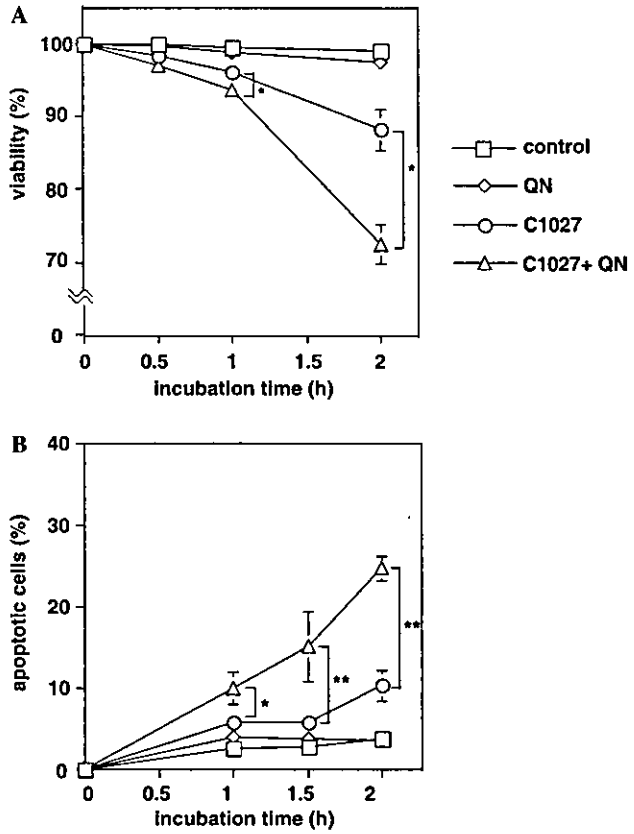

Fig. 2. Cell viability and apoptosis of HL-60 cells treated with C1027 and QN. Cells (5×10^5 cells/ml) were incubated with 50 pM C1027 and 1 μM QN in 2 ml medium at 37 °C. Control cells were incubated without C1027 and QN at 37 °C. At the indicated time, the percentages of trypan blue-positive cells (A) and cells showing condensed chromatin in the Hoechst 33258 and propidium iodide staining (B) were determined. Values represent means ± SD of three independent experiments. *$p < 0.05$, and **$p < 0.01$, statistically significant compared with C1027 alone.

Enhancing effect of QN on C1027-induced cellular DNA strand breaks

We analyzed DNA strand breaks in HL-60 cells treated with C1027 and QN using pulse field gel electrophoresis (Fig. 3). DNA fragments of 1–2 Mb scarcely appeared in the cells treated with 25 pM C1027 alone and were slightly enhanced by the addition of QN. C1027-induced DNA strand breaks at 50 pM were clearly enhanced by the addition of QN. QN alone did not induce cellular DNA strand breaks under the condition used.

Enhancing effect of QN on C1027-induced internucleosomal DNA fragmentation

We analyzed the effect of QN on DNA ladder formation in HL-60 cells treated with C1027. QN induced a significant increase in DNA ladder formation induced by C1027 from 0.5 μM, and most prominently at 1 μM (Fig. 4). At higher concentrations of QN (2 and 5 μM), the

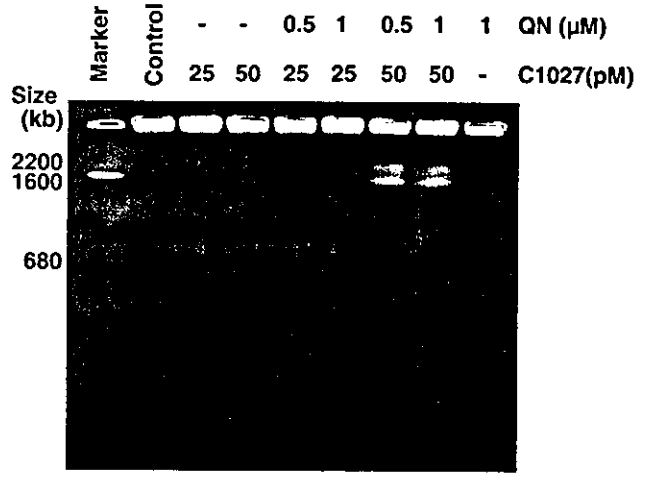

Fig. 3. Effect of QN on C1027-induced cellular DNA strand breaks in HL-60 cells. Cells (5×10^5 cells/ml) were treated with C1027 and QN in 2 ml medium for 10 min at 37 °C. Control cells were incubated without C1027 and QN for 10 min at 37 °C. The cells were prepared in agarose plugs, lysed, and subjected to pulse field gel electrophoresis through a 1% agarose gel, as described in Materials and methods. The gel was stained in ethidium bromide. Marker lane: size marker DNA (*Saccharomyces cerevisiae*).

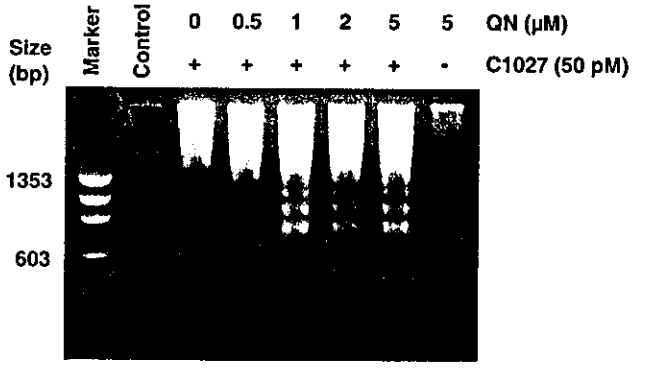

Fig. 4. Effect of QN on C1027-induced internucleosomal DNA fragmentation in HL-60 cells. Cells (5×10^5 cells/ml) were treated with 50 pM C1027 and 1 μM QN in 2 ml medium for 2 h at 37 °C. Control cells were incubated without C1027 and QN for 2 h at 37 °C. Cells were lysed and then DNA was extracted and analyzed by conventional electrophoresis as described in Materials and methods. Marker lane: size marker DNA (Φ-X174/*Hae*III digest).

formation of DNA ladders was decreased. QN alone formed little or no DNA ladder under the condition used.

Enhancing effect of QN on C1027-induced generation of H_2O_2 in HL-60 and HP100 cells

We observed peroxide generation in HL-60 and HP100 cells following treatment with C1027 and QN (Fig. 5). C1027 alone slightly increased peroxide generation when compared to the control in HL-60 cells. C1027-induced peroxide generation was significantly enhanced by the addition of QN in HL-60 cells. QN alone did not increase the peroxide generation. On the other hand, C1027 plus QN did not increase the peroxide generation in HP100 cells. This result indicates that the peroxide is mainly H_2O_2, because catalase activity in HP100 cells is much higher than that in HL-60 cells [26].

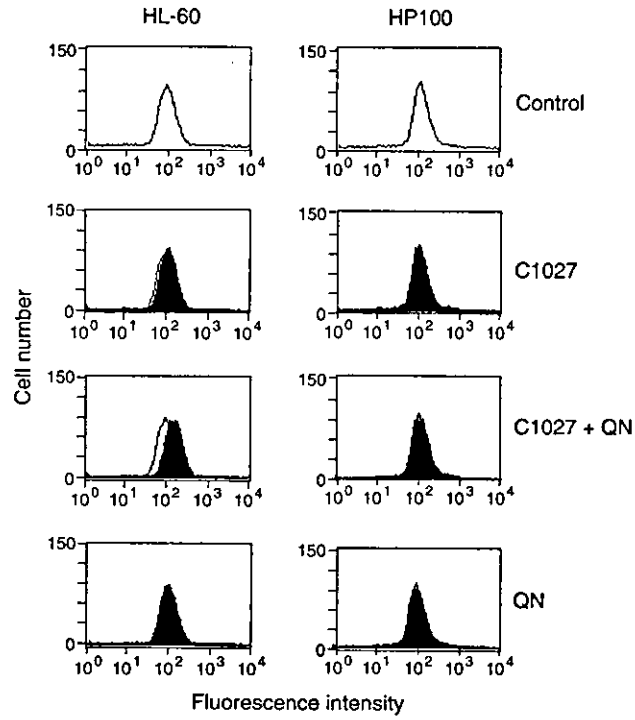

Fig. 5. Generation of peroxide in HL-60 and HP100 cells treated with C1027 and QN. Cells (5×10^5 cells/ml) were treated with 50 pM C1027, 1 μM QN and 5 μM DCFH-DA in 2 ml medium for 30 min at 37 °C. Control cells were incubated without C1027 and QN for 30 min at 37 °C. Following treatment, cells were analyzed on a flow cytometer (FACScan). The horizontal axis indicates the relative fluorescence intensity and the vertical axis designates cell numbers. Open peaks, distribution of the fluorescence intensity of the control.

Activation of caspase-3 in HL-60 cells treated with C1027 and the enhancing effect of QN

We measured caspase-3 activity in HL-60 cells treated with C1027 and QN using a fluorometric assay with DEVD-AFC as a substrate. C1027 alone slightly increased caspase-3 activation when compared with the control (Fig. 6). The addition of QN significantly enhanced C1027-induced caspase-3 activation ($p < 0.05$). QN alone did not increase caspase-3 activity.

Inhibitory effect of Bcl-2 on apoptosis in BJAB cells treated with C1027 and QN

We examined the effect of QN on C1027-induced apoptosis using BJAB cells by morphologic analysis. QN significantly enhanced C1027-induced apoptosis in BJAB/neo cells ($p < 0.05$) (Fig. 7). QN alone did not significantly increase the apoptotic cell number in BJAB/neo cells compared with control. C1027 plus QN-

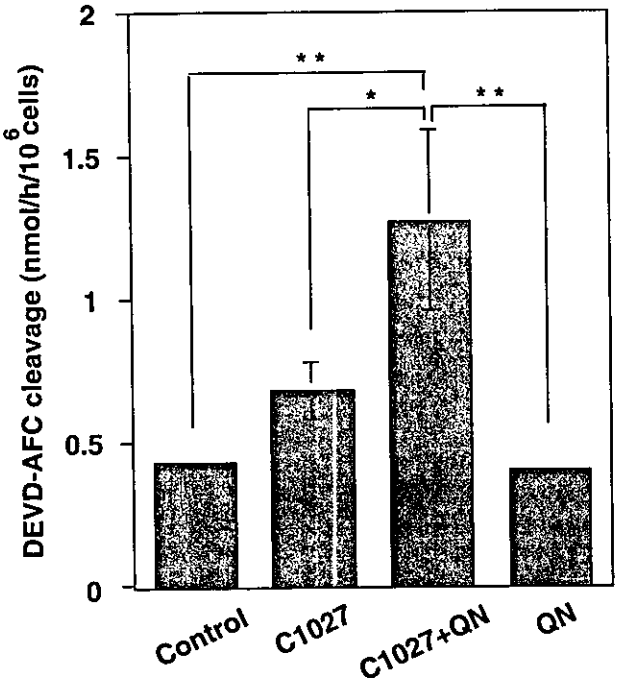

Fig. 6. Activation of caspase-3 in HL-60 cells treated with C1027 and/or QN. HL-60 cells (5×10^5 cells/ml) were treated with 50 pM C1027 and 1 μM QN in 2 ml medium for 2 h at 37 °C. Control cells were incubated without C1027 and QN for 2 h at 37 °C. Caspase-3 activity was measured by the cleavage of DEVD-AFC. Values represent means ± SD of three independent experiments. Significant difference was observed between the two groups using Scheffe's test ($*p < 0.05$; $**p < 0.01$).

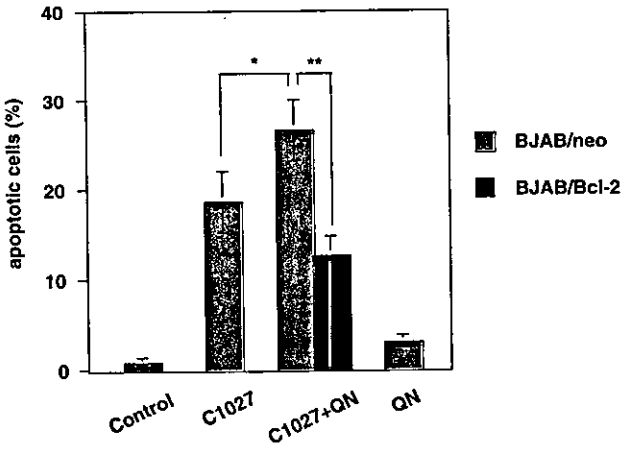

Fig. 7. Inhibitory effect of Bcl-2 on apoptosis in BJAB cells treated with C1027 and QN. BJAB/neo (shaded column) and BJAB/Bcl-2 (closed column) cells (5×10^5 cells/ml) were treated with 0.2 nM C1027 and 1 μM QN in 2 ml medium for 2 h at 37 °C. Control cells were incubated without C1027 and QN for 2 h at 37 °C. Percentage of apoptotic cells was determined by Hoechst 33258 and propidium iodide staining. Values represent means ± SD of three independent experiments. Significant difference was observed between the two groups using independent t test ($*p < 0.05$; $**p < 0.01$).

induced apoptosis was significantly inhibited in BJAB/Bcl-2 cells ($p < 0.01$), suggesting that this apoptosis was suppressed by Bcl-2 expression (Fig. 7).

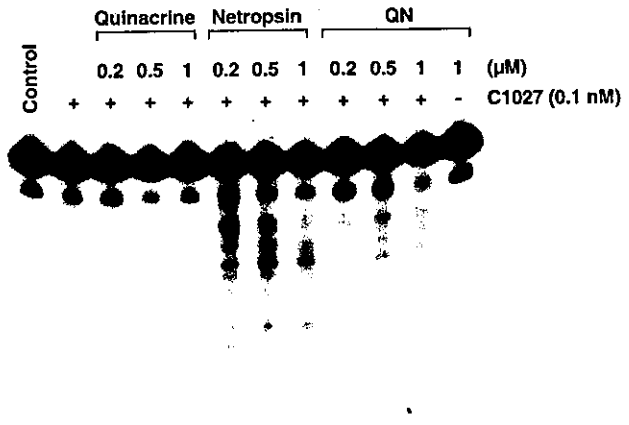

Fig. 8. Autoradiogram of the ^{32}P-5′-end-labeled DNA fragment cleaved by C1027 in the presence of DNA-binding ligands. The reaction mixture contained the 337-bp ^{32}P-5′-end-labeled DNA fragments of the human c-Ha-*ras*-1 proto-oncogene, calf thymus DNA (10 μM/base), indicated concentration of DNA-binding ligands, and 0.1 nM C1027 in 200 μl of 10 mM sodium phosphate buffer (pH 7.8) containing 5 μM DTPA. In the control, the reaction mixture did not contain C1027 and DNA-binding ligand. After incubation for 30 min at 37 °C, the treated DNA fragments were electrophoresed on an 8% polyacrylamide/8 M urea gel. The autoradiogram was obtained by exposing an X-ray film to the gel.

Enhancing effect of DNA-binding ligands on C1027-induced cleavage of isolated DNA

We investigated the effect of DNA-binding ligands on C1027-induced cleavage of ^{32}P-labeled DNA fragment obtained from the human c-Ha-*ras*-1 proto-oncogene. Quinacrine had no enhancing effect on C1027-induced DNA cleavage (Fig. 8). Netropsin enhanced the DNA cleavage more strongly than QN. QN alone formed no DNA cleavage under the condition used.

Site specificity of DNA cleavage induced by C1027 in the presence of QN

We investigated the relative intensity of DNA cleavage induced by C1027 in the presence and absence of QN, obtained by scanning the autoradiograms with a laser densitometer. C1027 alone induced double-stranded cleavage particularly at 5′-AAG-3′/3′-TTC-5′ (Fig. 9) and 5′-AAAA-3′/3′-TTTT-5′ sequences (data not shown) (cutting sites are underlined). Addition of QN changed the site specificity of DNA cleavage by C1027. The DNA cleavage at GC-rich sequences, particularly at the 5′-AGG-3′/3′-TCC-5′ sequence, was considerably enhanced by the addition of QN.

Discussion

We have studied the enhancing effects of DNA-binding ligands on DNA cleavage by antitumor drugs.

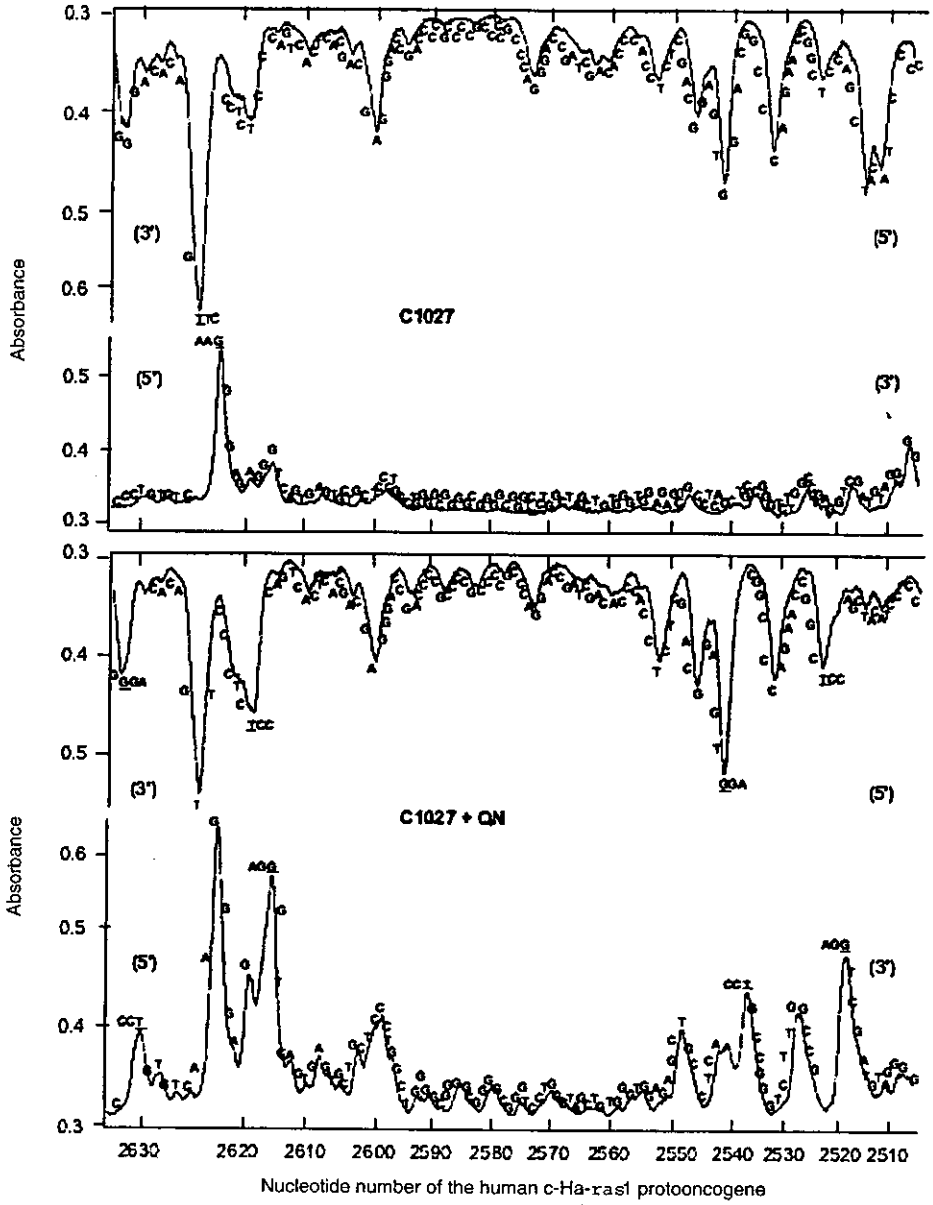

Fig. 9. Alteration in site specificity of C1027-induced DNA strand breaks by QN. The reaction mixture contained the 337-bp ^{32}P-5′- or ^{32}P-3′-end-labeled DNA fragments of the human c-Ha-*ras*-1 proto-oncogene, calf thymus DNA (10 μM/base), indicated concentration of QN and 0.1 nM C1027 in 200 μl of 10 mM sodium phosphate buffer (pH 7.8) containing 5 μM DTPA. After incubation for 30 min at 37 °C, the treated DNA fragments were electrophoresed as described in Fig. 8 legend. The relative amounts of DNA fragments were measured by scanning the autoradiogram with a laser densitometer (Personal Densitometer SI, Amarsham Biosciences).

Certain unfused aromatic cations dramatically amplified bleomycin-induced DNA cleavage, resulting in extensive enhancement of apoptosis [8]. Notably, the present study has shown that the newly synthesized DNA-binding ligand, QN, significantly enhanced both C1027-induced cytotoxicity and DNA ladder formation, suggesting that the enhanced cytotoxicity is due to induction of apoptosis. Quinacrine or netropsin alone did not affect the cytotoxicity of C1027. These results suggest that an effective DNA ligand, which is capable of amplifying the cytotoxicity of C1027, can be produced by the linkage of quinacrine and netropsin. Although QN and netropsin enhanced C1027-induced cleavage of isolated DNA fragments, only QN showed the enhancing effect on cytotoxicity of C1027. Quinacrine did not enhance DNA cleavage. It is reported that quinacrine highly distributes in tissue due to its high permeability to cell membrane [19]. Therefore, we consider that the quinacrine moiety facilitates the incorporation of QN into cells and the netropsin moiety is responsible for amplification of C1027-induced DNA cleavage, resulting in enhanced cytotoxicity. Although it has been reported that quinacrine, a phospholipase inhibitor, activates cytochrome *c*-dependent apoptotic signaling pathway [36], QN at the

concentration incapable of causing apoptosis was used in the present study. Thus, under this condition, the apoptotic pathway induced by the quinacrine moiety does not participate in QN-mediated enhancement of C1027-induced apoptosis.

It has been reported that C1027 is positioned inside the minor groove of duplex DNA, and the diradical species can abstract hydrogen atoms from deoxyriboses, resulting ultimately in DNA double-stranded breaks predominantly at 5′-TTT-3′/3′-AAA-5′, 5′-TAA-3′/3′-ATT-5′, 5′-TCT-3′/3′-AGA-5′, and 5′-TTA-3′/3′-AAT-5′ [16]. Additionally, this study revealed that C1027 alone cleaved DNA at 5′-AAG-3′/3′-TTC-5′ and 5′-AAAA-3′/3′-TTTT-5′ sequences. It is noteworthy that addition of QN changed the patterns of DNA strand breaks by C1027 and considerably enhanced the strand breaks at GC-rich sequences, particularly at 5′-AGG-3′/3′-TCC-5′ sequence, with a two-nucleotide 3′-stagger of the cleaved residues. We previously reported that distamycin A altered the site specificity of DNA cleavage by duocarmycin A [10]. This fact is explained by the report that distamycin A and duocarmycin A, both of which recognize DNA minor groove at AT-rich sequences, can form a heterodimer at GC-rich sequences in the relatively wider minor groove in a side-by-side arrangement [37]. These reports lead to an idea that C1027 may form a heterodimer with the netropsin moiety of QN, which fits snugly at GC-rich sequences in the minor groove rather than AT-rich sequences. Thus, the amplification of C1027-induced DNA cleavage at GC-rich sequences by QN may play an important role in enhancement of antitumor effect.

We showed that QN enhanced DNA strand breaks in the cells treated with C1027 at 10 min. This result suggests that amplification of DNA strand breaks may be an initial event of enhancement of apoptosis. Following DNA strand breaks, C1027-induced H_2O_2 generation and caspase-3 activation, which were significantly enhanced by the addition of QN. We previously reported that, in antitumor drug-induced apoptosis, DNA strand breaks lead to poly(ADP–ribose) polymerase hyperactivation and subsequent NAD^+ depletion, followed by the activation of NAD(P)H oxidase, which mediates H_2O_2 generation, followed by caspase-3 activation [4]. This pathway can reasonably explain the enhancement of C1027-induced apoptosis by QN.

Selective killing of tumor cells is an important goal for cancer therapeutics. It has been reported that C1027 provoked the retardation at G2/M phase followed by cell death in human hepatoma cells [38]. C1027-induced cell cycle arrest may show a selective effect against highly proliferating cancer cells rather than non-cancer cells. The present results show that C1027-induced selective killing of tumor cells could be enhanced by the concomitant use of QN. Therefore, QN may contribute to establishment of more effective chemotherapies with limited side effects.

As a method to approach a new chemotherapy to treat cancer more effectively and to reduce side effects, we have demonstrated that DNA cleavage induced by antitumor drugs was enhanced by DNA-binding ligands, which do not cause DNA damage [8–12]. In the present study, we have shown that apoptosis through C1027-induced DNA strand breaks could be significantly enhanced by the addition of QN, a newly synthesized DNA-binding ligand. Our findings may provide useful information for the design of DNA-binding ligands, which would raise a great clinical advantage.

Acknowledgment

We are grateful to Prof. Yukio Kubota, Department of Chemistry, Faculty of Science, Yamaguchi University, for providing us with QN.

References

[1] L.H. Hurley, Nat. Rev. Cancer 2 (2002) 188–200.
[2] S. Tada-Oikawa, S. Oikawa, M. Kawanishi, M. Yamada, S. Kawanishi, FEBS Lett. 442 (1999) 65–69.
[3] S.H. Kaufmann, W.C. Earnshaw, Exp. Cell Res. 256 (2000) 42–49.
[4] H. Mizutani, S. Tada-Oikawa, Y. Hiraku, S. Oikawa, M. Kojima, S. Kawanishi, J. Biol. Chem. 277 (2002) 30684–30689.
[5] C.J. Norbury, B. Zhivotovsky, Oncogene 23 (2004) 2797–2808.
[6] W.D. Wilson, F.A. Tanious, H.J. Barton, R.L. Wydra, R.L. Jones, D.W. Boykin, L. Strekowski, Anticancer Drug Des. 5 (1990) 31–42
[7] C. Helene, Curr. Opin. Biotechnol. 4 (1993) 29–36.
[8] S. Kawanishi, S. Oikawa, M. Kawanishi, H. Sugiyama, I. Saito, L Strekowski, W.D. Wilson, Biochemistry 39 (2000) 13210–13215.
[9] K. Yamamoto, S. Kawanishi, Biochem. Biophys. Res. Commun. 183 (1992) 292–299.
[10] K. Yamamoto, H. Sugiyama, S. Kawanishi, Biochemistry 32 (1993) 1059–1066.
[11] Y. Hiraku, S. Oikawa, K. Kuroki, H. Sugiyama, I. Saito, S. Kawanishi, Biochem. Pharmacol. 61 (2001) 351–356.
[12] Y. Hiraku, S. Kawanishi, Biochem. Biophys. Res. Commun. 239 (1997) 134–138.
[13] J.S. Liu, S.R. Kuo, X. Yin, T.A. Beerman, T. Melendy, Biochemistry 40 (2001) 14661–14668.
[14] Y.S. Zhen, X.Y. Ming, B. Yu, T. Otani, H. Saito, Y. Yamada, J. Antibiot. 4 (1989) 1294–1298.
[15] Y. Sugiura, T. Matsumoto, Biochemistry 32 (1993) 5548–5553.
[16] X.J. Xu, Y.S. Zhen, I.H. Goldberg, Biochemistry 33 (1994) 5947–5954.
[17] T. Hatayama, I.H. Goldberg, M. Takeshita, A.P. Grollman, Proc. Natl. Acad. Sci. USA 75 (1978) 3603–3607.
[18] H. Maeda, K. Edo, N. Ishida, Neocarzinostatin, The Past, Present, and Future of an Anticancer Drug, Springer-Verlag, Tokyo, 1997.
[19] N.H. Dubin, D.A. Blake, M.C. DiBlasi, T.H. Parmley, T.M. King, Fertil. Steril. 38 (1982) 735–740.
[20] L. Rivas, A. Murza, S. Sanchez-Cortes, J.V. Garcia-Ramos, J. Biomol. Struct. Dyn. 18 (2000) 371–383.
[21] K.M. Stuhlmeier, Biochim. Biophys. Acta 1524 (2001) 57–65.
[22] C. Zimmer, Prog. Nucleic Acid Res. Mol. Biol. 15 (1975) 285–318.
[23] S. Neidle, L.H. Pearl, J.V. Skelly, Biochem. J. 243 (1987) 1–13.
[24] J.W. Lown, K. Krowicki, J. Org. Chem. 50 (1985) 3774–3779.
[25] Y. Kubota, S. Kawamura, R. Uchida, Nucleic Acids Symp. Ser. 42 (1999) 247–248.

[26] I. Kasugai, M. Yamada, Leuk. Res. 16 (1992) 173–179.
[27] S. Yoshimura, Y. Banno, S. Nakashima, K. Takenaka, H. Sakai, Y. Nishimura, N. Sakai, S. Shimizu, Y. Eguchi, Y. Tsujimoto, Y Nozawa, J. Biol. Chem. 273 (1998) 6921–6927.
[28] K. Ito, K. Yamamoto, S. Kawanishi, Biochemistry 31 (1992) 11606–11613.
[29] Y. Hiraku, S. Kawanishi, Cancer Res. 56 (1996) 5172–5178.
[30] J. Xiang, D.T. Chao, S.J. Korsmeyer, Proc. Natl. Acad. Sci. USA 93 (1996) 14559–14563.
[31] K. Yamamoto, S. Kawanishi, J. Biol. Chem. 266 (1991) 1509–1515.
[32] S. Kawanishi, K. Yamamoto, Biochemistry 30 (1991) 3069–3075.
[33] D.J. Capon, E.Y. Chen, A.D. Levinson, P.H. Seeburg, D.V. Goeddel, Nature 302 (1983) 33–37.
[34] S. Oikawa, S. Kawanishi, in: N. Taniguchi, J.M.C. Gutteridge (Eds.), Experimental Protocols for Reactive Oxygen and Nitrogen Species, Oxford University Press, New York, 2000, pp. 229–235.
[35] A.M. Maxam, W. Gilbert, Methods Enzymol. 65 (1980) 499–560.
[36] A.A. Fasanmade, E.D. Owuor, R.P. Ee, D. Qato, M. Heller, A.N. Kong, Arch. Pharm. Res. 24 (2001) 126–135.
[37] H. Sugiyama, C. Lian, M. Isomura, I. Saito, A.H. Wang, Proc. Natl. Acad. Sci. USA 93 (1996) 14405–14410.
[38] Y.X. Liang, W. Zhang, D.D. Li, H.T. Liu, P. Gao, Y.N. Sun, R.G. Shao, World J. Gastroenterol. 10 (2004) 2632–2636.

Available online at www.sciencedirect.com
SCIENCE DIRECT®
Chemico-Biological Interactions 150 (2004) 271–281
Chemico-Biological Interactions
www.elsevier.com/locate/chembioint

Metabolic activation of carcinogenic ethylbenzene leads to oxidative DNA damage

Kaoru Midorikawa[a], Takafumi Uchida[b], Yoshinori Okamoto[b], Chitose Toda[b], Yoshie Sakai[b], Koji Ueda[b], Yusuke Hiraku[a], Mariko Murata[a], Shosuke Kawanishi[a,*], Nakao Kojima[b,*]

[a] *Department of Environmental and Molecular Medicine, Mie University School of Medicine, 2-174 Edobashi, Tsu, Mie 514-8507, Japan*
[b] *Faculty of Pharmacy, Meijo University, 150 Yagotoyama, Nagoya 468-8503, Japan*

Received 24 July 2004; received in revised form 27 September 2004; accepted 27 September 2004

Abstract

Ethylbenzene is carcinogenic to rats and mice, while it has no mutagenic activity. We have investigated whether ethylbenzene undergoes metabolic activation, leading to DNA damage. Ethylbenzene was metabolized to 1-phenylethanol, acetophenone, 2-ethylphenol and 4-ethylphenol by rat liver microsomes. Furthermore, 2-ethylphenol and 4-ethylphenol were metabolically transformed to ring-dihydroxylated metabolites such as ethylhydroquinone and 4-ethylcatechol, respectively. Experiment with ^{32}P-labeled DNA fragment revealed that both ethylhydroquinone and 4-ethylcatechol caused DNA damage in the presence of Cu(II). These dihydroxylated compounds also induced the formation of 8-oxo-7,8-dihydro-2′-deoxyguanosine in calf thymus DNA in the presence of Cu(II). Catalase, methional and Cu(I)-specific chelator, bathocuproine, significantly ($P<0.05$) inhibited oxidative DNA damage, whereas free hydroxyl radical scavenger and superoxide dismutase did not. These results suggest that Cu(I) and H_2O_2 produced via oxidation of ethylhydroquinone and 4-ethylcatechol are involved in oxidative DNA damage. Addition of an endogenous reductant NADH dramatically enhanced 4-ethylcatechol-induced oxidative DNA damage, whereas ethylhydroquinone-induced DNA damage was slightly enhanced. Enhancing effect of NADH on oxidative DNA damage by 4-ethylcatechol may be explained by assuming that reactive species are generated from the redox cycle. In conclusion, these active dihydroxylated metabolites would be involved in the mechanism of carcinogenesis by ethylbenzene.

Keywords: Ethylbenzene; Metabolic activation; Oxidative DNA damage; Carcinogenesis; Hydrogen peroxide; Copper

1. Introduction

Ethylbenzene is contained in crude petroleum, mobile fuel, paint solvent and cigarette smoke. Because of

* Corresponding authors. Tel.: +81 59 231 5011 (S. Kawanishi)/+81 52 832 1781 (N. Kojima); fax: +81 59 231 5011 (S. Kawanishi)/+81 52 834 8090 (N. Kojima).
E-mail addresses: kawanisi@doc.medic.mie-u.ac.jp (S. Kawanishi), kojiman@ccmfs.meijo-u.ac.jp (N. Kojima).

0009-2797/$ – see front matter © 2004 Elsevier Ireland Ltd. All rights reserved.
doi:10.1016/j.cbi.2004.09.020

its high volatility, ethylbenzene is widely distributed in the environment. Ethylbenzene has been issued as an air pollutant, especially an indoor pollutant. Ethylbenzene is readily absorbed via inhalation [1–3] as well as oral administration [4]. Ethylbenzene causes carcinoma in the kidney and testis of rats, and in the lung and liver of mice by inhalation [5]. Thus, ethylbenzene has been categorized as a group 2B carcinogen (possibly carcinogenic to humans) by the International Agency of Research on Cancer [6]. However, the mechanism of carcinogenesis by ethylbenzene remains to be clarified. Ethylbenzene itself has no mutagenic activity [6]. Most of the Ames test-negative chemicals exert their carcinogenicity via oxidative DNA damage [7–9]. In the present study, we examined whether the metabolites of ethylbenzene are capable of causing DNA damage through generation of reactive oxygen species. A main metabolite of ethylbenzene, 1-phenylethanol, induced renal tubular adenomas at high dose in male rats [10]. In addition, alternative pathways including ring-hydroxylation are also possible [11]. The resulting metabolites might be responsible for the ethylbenzene-mediated carcinogenesis.

To confirm this hypothesis, we analyzed ethylbenzene metabolites formed by rat liver microsomes and their ability to cause oxidative DNA damage. The metabolites were identified by high performance liquid chromatography (HPLC) and gas chromatography/mass spectrometry (GC/MS). We investigated the ability of ethylbenzene metabolites to induce DNA damage using ^{32}P-labeled DNA fragments obtained from the human *p53* tumor suppressor gene. This gene is known to be the most important target for chemical carcinogens [12]. Moreover, mutations in the *p53* gene have been frequently found in cancer patients [13]. Effect of these metabolites on the formation of 8-oxo-7,8-dihydro-2′-deoxyguanosine (8-oxodG), a characteristic oxidative product of DNA, was analyzed using an HPLC equipped with an electrochemical detector (ECD).

2. Materials and methods

2.1. Chemicals

Ethylbenzene, acetophenone, 2-ethylphenol and 4-ethylphenol were purchased from Aldrich Chemical (Milwaukee, WI). 1-Phenylethanol was from Fluka Chemie GmbH (Buchs, Switzerland). 4-Ethylcatechol (EC) was from Tokyo Kasei Kogyo (Tokyo, Japan). Ethylhydroquinone (EHQ), bis(trimethylsilyl)trifluoroacetamide (BSTFA) and calf thymus DNA were from Sigma Chemical (St. Louis, MO). Glucose 6-phosphate dehydrogenase, β-nicotinamide-adenine dinucleotide phosphate ($NADP^+$), D-glucose 6-phosphate, dimethyl sulfoxide (DMSO) and superoxide dismutase (SOD) were from Wako Pure Chemical (Osaka, Japan). Nuclease P_1 was from Yamasa Shoyu (Choshi, Chiba, Japan). Calf intestine alkaline phosphatase (CIP) was purchased from Roche Diagnostics (Mannheim, Germany). Phenobarbital was from Hoei (Osaka, Japan). Ethylbenzene, 2-ethylphenol, 4-ethylphenol, EHQ and EC were of the highest purity available (>95%). Other chemicals used were of the highest quality commercially available.

2.2. Preparation of rat liver microsomes

We prepared microsomes from the liver of male Sprague–Dawley rats (5 weeks of age, Clea Japan, Tokyo, Japan) as described previously [14]. These rats were given oral administration of phenobarbital (60 mg/kg body weight) daily for 3 days before use. The livers of rats were excised from exsanguinated rats and immediately perfused with 1.15% KCl. The livers were homogenized in four volumes of the KCl solution using a homogenizer. The microsomal fraction was obtained from the homogenate by successive centrifugation at 9000 × *g* for 20 min and 105,000 × *g* for 60 min. The fraction was washed by resuspension in the same solution and recentrifugation. The pellets of microsomes were resuspended in 1 ml of the solution for 1 g of liver. Protein amount was quantified by the Bradford method using Biorad protein assay dye reagent (Biorad, Hercules, CA). Quantity of cytochrome P450 (0.68 ± 0.04 nmol/mg protein) was determined by the method of Omura and Sato [15].

2.3. Microsomal reaction

Microsomal reaction mixture contains 2 mg/ml of microsomal protein, 1 mM $NADP^+$, 10 mM glucose 6-phosphate, 1 unit/ml of glucose 6-phosphate dehydrogenase and 10 mM $MgCl_2$ in 1 ml of 100 mM

phosphate buffer (pH 7.4). Substrate (ethylbenzene, 2-ethylphenol or 4-ethylphenol) dissolved in DMSO was added into the mixture (5 mM, final concentration of substrate) and incubated for 30 min at 37 °C. After incubation, 200 mM HCl was added and the products were extracted with diethyl ether three times. The pooled diethyl ether extract was dehydrated with sodium sulfate anhydride and evaporated.

2.4. HPLC analysis

The dried extract of microsomal reaction mixture was dissolved in 40% methanol–water containing 0.1% trifluoroacetic acid (TFA) and applied to an HPLC system (LC-VP, Shimadzu, Kyoto, Japan) equipped with a diode array detector and Develosil packed column (4.6 mm i.d. × 250 mm, Nomura Chemical, Aichi, Japan) and eluted with 40% methanol–water containing 0.1% TFA at a flow rate of 1 ml/min at 40 °C.

2.5. GC/MS analysis

For GC/MS analysis, the extract was dissolved in 100 μl of methanol. Some compounds, such as EHQ and EC, were purified by HPLC, evaporated and incubated for 30 min at 60 °C in BSTFA for a derivatization before the analysis. The samples were injected into a GC (HP 6890 GC System Plus, Agilent Technologies, Palo Alto, CA) equipped with a MS (JMS-700 MStation, JEOL, Tokyo, Japan), using electron impact ionization at 70 eV. Helium was used as carrier gas at a flow rate of 0.5 ml/min. Temperature of injector, interface and ion source was 200 °C. The temperature program for an HP Ultra 2 column (0.2 mm i.d. × 25 m × 0.33 μm film thickness, Agilent Technologies) was as follows: 40 °C (2 min isothermal), 40–120 °C (2 °C/min), and 120 °C (5 min isothermal). For derivatized compounds, temperature of injector, interface and ion source was 250 °C, and the temperature program was as follows: 70 °C (2 min isothermal), 70–280 °C (10 °C/min), and 280 °C (5 min isothermal).

2.6. Detection of damage to ^{32}P-5′-end labeled DNA

DNA fragments obtained from the human *p53* tumor suppressor gene [16] containing exons were prepared, as described previously [17]. The 5′-end labeled 650 bp fragment (*Hin*dIII* 13972–*Eco*RI* 14621) was obtained by dephosphorylation with CIP and rephosphorylation with [γ-^{32}P]ATP and T_4 polynucleotide kinase. The asterisk (*) indicates ^{32}P-labeling. The 650 bp fragment was further digested with *Apa*I to obtain a singly labeled 443 bp fragment (*Apa*I 14179–*Eco*RI* 14621). The standard reaction mixtures (1.5 ml in an Eppendorf microtube) containing ethylbenzene metabolites, ^{32}P-5′-end labeled DNA fragments, calf thymus DNA (50 μM/base), 100 μM NADH and 20 μM $CuCl_2$ in 200 μl of 10 mM sodium phosphate buffer (pH 7.8) containing 5 μM DTPA were incubated at 37 °C for 1 h. Then, the DNA fragments were treated in 10% (v/v) piperidine at 90 °C for 20 min. The treated DNA was electrophoresed on an 8% polyacrylamide/8 M urea gel. The autoradiogram was obtained by exposing X-ray film to the gel.

2.7. Analysis of 8-oxodG formation in calf thymus DNA

Calf thymus DNA (50 μM/base) was incubated with ethylbenzene metabolites, and 20 μM $CuCl_2$ in 4 mM sodium phosphate buffer (pH 7.8) for 1 h at 37 °C. In a certain experiment, 100 μM NADH was added. After ethanol precipitation, DNA was digested to the nucleosides with nuclease P_1 and CIP, and then 8-oxodG content was measured with an HPLC-ECD as described previously [18]. To examine the reactive species involved in 8-oxodG formation, scavengers (ethanol, methional, SOD and catalase) and a metal chelator (bathocuproine) were added before addition of ethylbenzene metabolites to reaction mixtures. The reaction mixtures were incubated and 8-oxodG content was measured as described above.

2.8. Detection of O_2^- derived from ethylbenzene metabolites

The amount of O_2^- generated by the reaction of EHQ or EC with Cu(II) was determined by the measurement of cytochrome *c* reduction. The reaction mixture containing 40 μM ferricytochrome *c*, 100 μM EHQ or EC, 2.5 μM DTPA in 1 ml of

10 mM sodium phosphate buffer (pH 7.8) with or without SOD (100 units) was incubated at 37 °C. Maximum absorption of reduced cytochrome *c* at 550 nm ($\varepsilon_{550} = 21{,}100\,M^{-1}\,cm^{-1}$) was recorded at 1 min intervals for 6 min, using a UV–visible absorption spectrophotometer (Hitachi 228A, Tokyo, Japan). The content of O_2^- was calculated by subtracting absorbance with SOD from that without SOD.

2.9. Measurement of Cu(I)–bathocuproine complex in the reaction of ethylbenzene metabolites and Cu(II)

Cu(I) was quantified by measuring characteristic absorption of Cu(I)–bathocuproine complex at 480 nm [19]. The reaction mixture containing 200 μM bathocuproine, 50 μM $CuCl_2$ and a test compound (EHQ or EC, 0–40 μM) dissolved in DMSO was analyzed by a spectrophotometer (Hitachi) immediately after addition of these reagents. The amount of Cu(I) was calculated using molar absorbance coefficient of the complex ($\varepsilon_{480} = 13{,}900\,M^{-1}\,cm^{-1}$).

3. Results

3.1. Metabolism of ethylbenzene by rat liver microsomes

Ethylbenzene was treated with rat liver microsomes and the metabolites were analyzed by HPLC and GC/MS. As side chain-oxidized metabolites, 1-phenylethanol and acetophenone were detected (Fig. 1). 2-Ethylphenol and 4-ethylphenol were detected as benzene ring-hydroxylated metabolites (Fig. 1). Approximately 3% of ethylbenzene was converted to 1-phenylethanol, and smaller amounts of 2-ethylphenol (0.0048%) and 4-ethylphenol (0.014%) were generated under the conditions used. The major peaks, which appeared before the retention time of 5 min, are attributed to microsomal components rather than ethylbenzene metabolites (Fig. 1). HPLC retention times and UV spectra of four metabolites were consistent with those of each authentic compound. Moreover, structures of these metabolites were confirmed by GC/MS analysis as estimated in the HPLC analysis (data not shown).

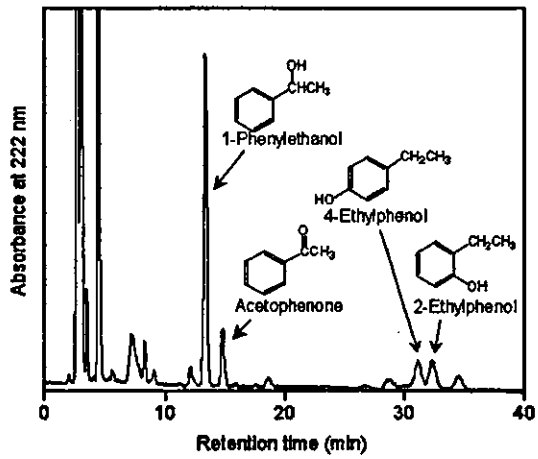

Fig. 1. HPLC profile of ethylbenzene metabolites formed by phenobarbital-treated rat liver microsomes. The conditions for the microsomal reaction and HPLC are as described in Section 2. Peaks without arrows are observed even in the absence of ethylbenzene.

3.2. 2-Ethylphenol and 4-ethylphenol-derived ethylbenzene metabolites

When 2-ethylphenol and 4-ethylphenol were treated with microsomes, ethylhydroquinone and 4-ethylcatechol were detected, respectively. Identification of these metabolites was estimated by the identical HPLC retention time and UV spectrum to that of each authentic standard (Fig. 2A and B) and confirmed by GC/MS analysis (data not shown). The major peaks, which appeared before 5 min in Fig. 2A, are attributed to microsomal components rather than ethylbenzene metabolites. The peak near 10 min in Fig. 2B is attributed to an unknown metabolite yet to be identified.

3.3. Damage to ^{32}P-labeled DNA fragments by ethylbenzene metabolites in the presence of NADH and Cu(II)

As shown in Fig. 3, both EHQ and EC induced DNA damage in the presence of Cu(II). The intensity of DNA damage increased with increasing concentrations of the metabolites (Fig. 3). Addition of an endogenous reductant NADH enhanced DNA damage by EHQ slightly. On the other hand, EC-induced DNA damage was dramatically enhanced by the addition of NADH (Fig. 3).

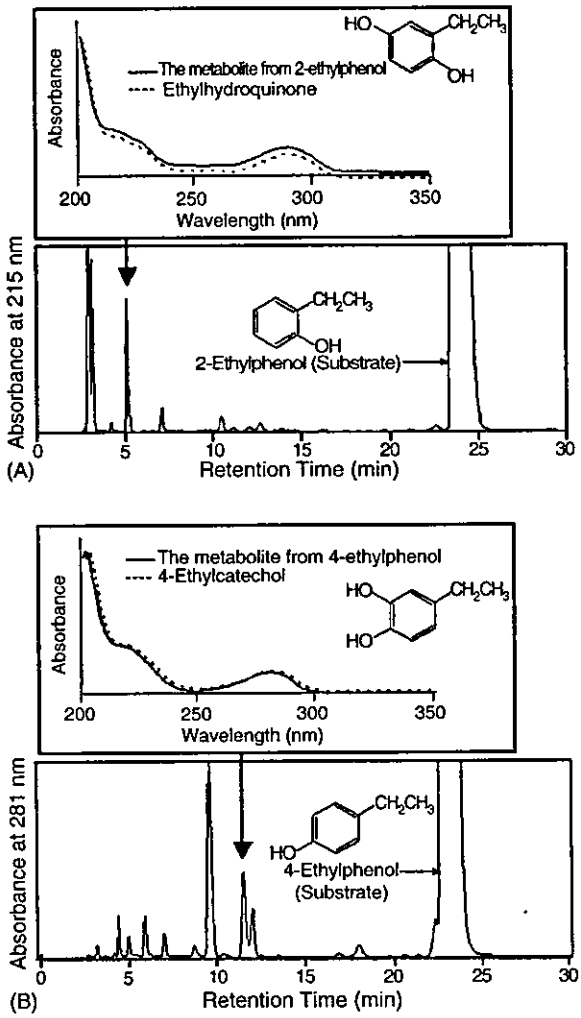

Fig. 2. HPLC profiles of 2-ethylphenol, 4-ethylphenol and their metabolites and UV spectra of the metabolites. The conditions for the microsomal reaction and HPLC are as described in Section 2. (Bottom) HPLC profiles of 2-ethylphenol (A) and 4-ethylphenol metabolites (B); (top) UV spectra of EHQ (A) and EC (B).

3.4. Formation of 8-oxodG in calf thymus DNA by ethylbenzene metabolites

Ethylbenzene metabolites, EHQ and EC, induced 8-oxodG formation in calf thymus DNA in the presence of Cu(II) in a dose-dependent manner (Fig. 4A and B). EHQ generated approximately two-fold larger amount of 8-oxodG compared with EC. Furthermore, EC-induced 8-oxodG formation increased three- to four-fold by the addition of NADH (Fig. 4B). In the case of EHQ, a slight increase in 8-oxodG formation was observed by the addition of NADH (Fig. 4A). When Cu(II) was omitted, the amounts of 8-oxodG induced by EHQ and EC were similar to the negative control (data not shown). Other ethylbenzene metabolites, 1-phenylethanol, acetophenone, 2-ethylphenol and 4-ethylphenol, did not exert 8-oxodG formation activity, under the conditions used (data not shown).

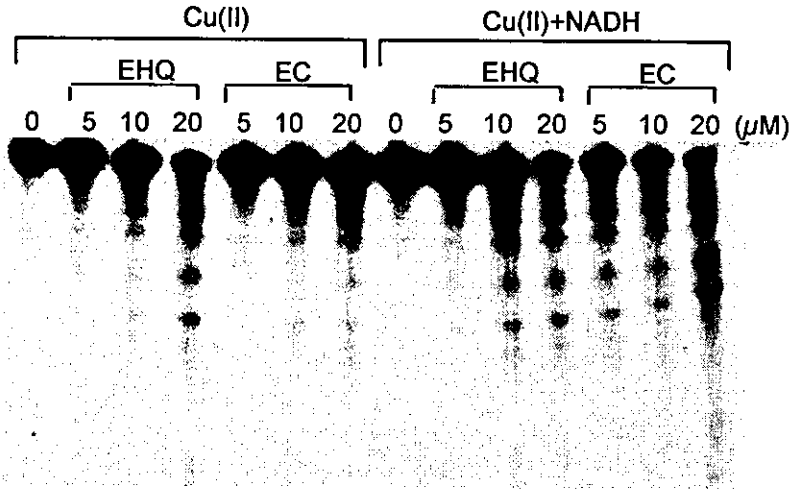

Fig. 3. Autoradiogram of ^{32}P-labeled DNA fragments incubated with ethylbenzene metabolites in the presence of NADH and Cu(II). The reaction mixtures containing each ethylbenzene metabolite (concentration as indicated), ^{32}P-5′-end labeled 443 bp DNA fragments, calf thymus DNA (50 μM/base), 100 μM NADH and 20 μM $CuCl_2$ in 200 μl of 10 mM sodium phosphate buffer (pH 7.8) containing 5 μM DTPA were incubated at 37 °C for 1 h. After the incubation, the DNA fragments were treated with hot piperidine, and electrophoresed on an 8% polyacrylamide/8 M urea gel. The autoradiogram was obtained by exposing X-ray film to the gel.

3.5. Effects of radical scavengers on the formation of 8-oxodG induced by ethylbenzene metabolites

To identify the reactive species responsible for DNA damage, we investigated the inhibitory effect of reactive oxygen species scavengers and Cu(I)-specific chelator bathocuproine on the 8-oxodG formation induced by EHQ and EC (Fig. 5). Typical hydroxyl radical scavenger ethanol did not show an inhibitory effect on 8-oxodG formation. Catalase significantly inhibited 8-oxodG formation in both cases. Relatively strong inhibition was observed with methional, a wide range scavenger, which reacts with various less reactive species other than hydroxyl radical. In addition, Cu(I)-specific chelator bathocuproine completely suppressed the 8-oxodG for-

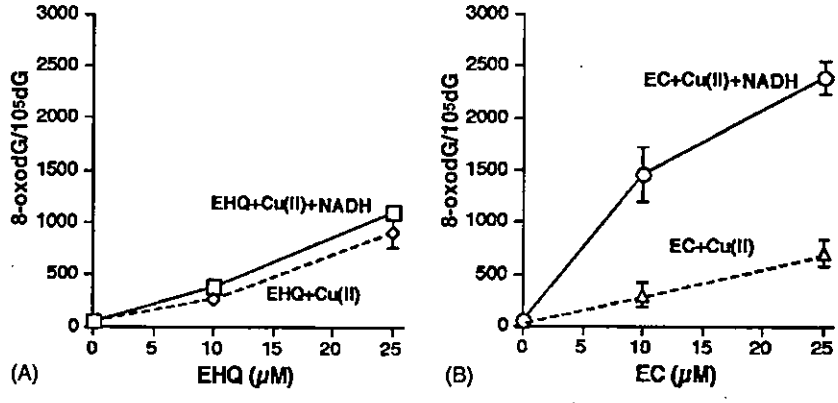

Fig. 4. Formation of 8-oxodG induced by EHQ or EC in the presence of Cu(II). Reaction mixture contained calf thymus DNA (50 μM/base), 20 μM $CuCl_2$, 100 μM NADH and EHQ (A) or EC (B) in 4 mM sodium phosphate buffer (pH 7.8) containing 5 μM DTPA. The reaction and measurement were performed as described in Section 2. Results were obtained from two independent experiments. Values are expressed as means ± S.D.